Nonlinear dynamics of a freely localized microwave discharge in an electromagnetic wave beam

A. L. Vikharev, V. B. Gil'denburg, S. V. Golubev, B. G. Eremin, O. A. Ivanov, A. G. Litvak, A. N. Stepanov, and A. D. Yunakovskiĭ

Institute of Applied Physics, Academy of Sciences of the USSR

(Submitted 18 August 1986)
Zh. Eksp. Teor. Fiz. **94**, 136–145 (April 1988)

A theoretical and experimental study is reported of the structure and dynamics of nonequilibrium microwave discharges produced in different gases by a quasioptical wave beam. Analysis of the data obtained by open-shutter and high-speed photography suggests that there are three types of discharge structure (diffuse, multiplasmoid, and filamentary) that succeed one another as the pressure increases. The experimental data are in satisfactory agreement with the numerically computed initial stages of the discharge and with the theory of ionization and field instabilities.

1. Advances in the development of sources of strong electric field (both static and rapidly varying) have always been accompanied by applications to electrical discharges in gases. This has led to the development of research into high-frequency inductive and capacitive discharges and, subsequently, microwave discharges in waveguides used in radar systems. There have also been clear benefits in another branch of nonlinear optics: even the very early experiments with powerful lasers demonstrated the possibility of optical breakdown (laser spark) and of hot plasmas in focused light beams, which has opened up essentially new avenues for research into controlled thermonuclear fusion.

Recent years have seen a resurgence of interest in another type of gas discharge, namely, the freely-localized nonequilibrium microwave discharge in a quasioptical beam of electromagnetic waves, which has become possible since the advent of powerful generators of microwave radiation. This type of discharge is a new and interesting phenomenon in nonlinear physics that has attracted considerable attention because of its possible applications to the production and utilization of chemically active nonequilibrium plasma with a high degree of purity (because of the absence of electrodes). The structure and dynamics of this discharge are determined by very unusual nonlinear electrodynamic processes[1–3] that may be looked upon as relatively poorly studied ionization analogs of well-known nonlinear processes in collisionless plasmas.

In previous experiments, this type of discharge was usually produced either at high pressure,[4–7] so that the electron collision frequency ν was greater than the field frequency ω, and gas dynamics and heating were the most important questions that had to be examined (rather than plasma electrodynamics), or by short microwave pulses[8–10] ($\tau_p \lesssim 10^{-6}$) that confined such studies to the characteristics of the primary breakdown in which many important nonlinear processes had not yet developed. The present paper is mostly devoted to an experimental study of the more important aspects of the space-time evolution of the self-sustaining nonequilibrium microwave discharge produced by a converging wave beam in low and intermediate pressure gases in which the electron temperature is much higher than the effective temperature of the molecules. The source of radiation was a gyrotron producing relatively powerful and long pulses of millimeter-wavelength radiation, which enabled us to investigate in detail the nonlinear dynamics of freely localized discharges in a wide range of gas density, and to establish many important properties of the interaction between the radiation and the gas-discharge plasma produced by it. The experimental data are compared with numerical calculations on the initial stages of the evolution of the discharge and with the predictions of the theory of small-scale ionization and field instabilities.

2. The microwave radiation produced by the gyrotron was transformed into a Gaussian beam of linearly polarized electromagnetic waves, which was directed into an echo-free vacuum chamber. The wavelength of the electromagnetic waves was $\lambda = 8$ nm, the pulse length was $\tau_i \simeq 100$ μs, and the peak power in the beam was $P \simeq 100$ kW. The transverse and longitudinal dimensions of the focal region in the undisturbed wave beam (at the point at which the intensity fell by a factor of e) where, respectively, $a \simeq 1.5$ cm and $l \simeq ka^2 \simeq 17$ cm ($ka \simeq 10$, $kl \simeq 100$, $k = \omega/c = 2\pi/\lambda$). The chamber was filled with technical grade nitrogen, helium, or argon (the impurity concentration was less than 1%). The discharge was struck in the focal region of the beam at a substantial distance from the chamber walls at pressures in the range $p = 0.1$–600 torr in helium and argon and $p = 0.3$–70 torr in nitrogen.

Discharge dynamics and structure were investigated mostly by examining plasma emission photographs. Equipment employed included a photographic camera and the LVE-1B and FER-2 systems incorporating image convertors[11] and operating in open-shutter and single-frame modes. The time-stretching LVE-1B system was modified to work with the multistage UMI-93Sh image convertor with a multiple-slit photocathode, so that the discharge could be photographed during the microwave pulse (nine frames at intervals of 2–32 μs with an exposure of 0.2 μs). The optical scan time of the photoelectron recorder FER-2 was increased to 50 μs).

The discharge was photographed in two mutually perpendicular projections, i.e., on a plane containing the beam axis parallel to the electric field (the E plane) and on the plane containing the same axis, but parallel to the magnetic field (the H plane). Whenever the spatial structure of the discharge was not too complicated, the photographic methods were augmented by measurements of electron density, which was determined from the frequency shift of an open resonator inserted into the chamber. The resonator was excited at the wavelength of $\lambda_0 = 4$ mm and consisted of two

 0038-5646/88/040724-05$04.00

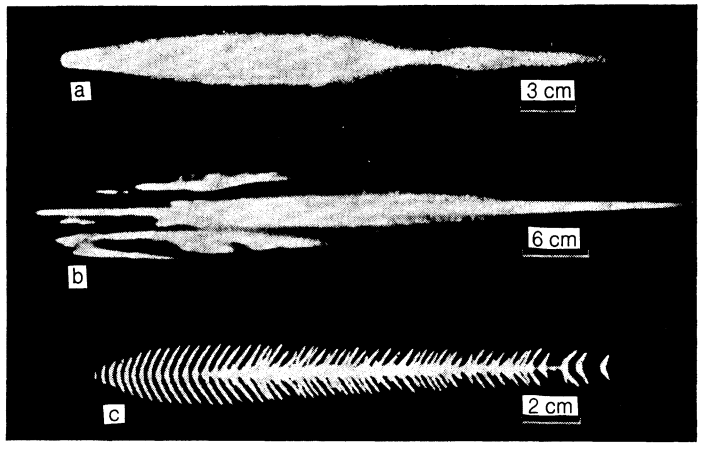

FIG. 1. Open-shutter photographs of a helium discharge, recorded in the E plane: a—$p = 5$ torr, b—100 torr, c—600 torr. The microwave beam propagates from left to right.

spherical mirrors, with the beam axis passing between them. The method employed (see Ref. 12) ensured that the electron density could be measured in the range 10^{11}–2×10^{13} cm^{-3} with a spatial resolution of about 1 cm, averaging time interval 1 μs, and minimum time interval between successive measurements in a given breakdown pulse of about 10–15 μs.

3. When the microwave power exceeded a certain threshold, there was a pressure range (density range) in which a discharge was struck in the focal region of the beam. The overall appearance of the discharge structure was significantly pressure dependent. The observed integrated emission showed the presence of three types of structure that succeeded one another as the pressure was raised: (1) continuous (diffuse) emission at low pressures, (2) bright bands parallel to the beam axis and perpendicular to the electric field **E** at intermediate pressures, and (3) bright filaments parallel to **E** at high pressures. The corresponding integrating photographs of the discharge in the E plane are shown in Fig. 1 in the case of helium. Transitions from the first type of structure to the second and from the second to the third are found to occur for nitrogen pressures $p_1 \simeq 3$–5 torr and $p_2 \simeq 40$–50 torr, and for helium pressures $p_1 \simeq 10$–20 torr and $p_2 \simeq 100$–150 torr. In argon, the second structure type was not observed: a transition from type one to type three structure was observed for pressures between 30 and 40 torr.

The main stages of the evolution of the discharge were identified by investigating the discharge dynamics by photorecording techniques. They were: (1) the onset of breakdown near the focal plane, (2) the displacement of the ionization front (principal maximum of the breakdown wave) in the opposite direction to that of the incident radiation, accompanied by the formation of a quasiuniform plasma column behind this front, and (3) the appearance of secondary traveling ionization waves and small-scale fragmentation of the resulting structures (in the corresponding pressure ranges) in the direction parallel or perpendicular to **E**.

4. The motion of the ionization region against the incident radiation is a well-known phenomenon, typical of discharges struck in different frequency ranges.[10,13] In self-sustaining microwave discharges, the principal mechanism responsible for this motion is the breakdown wave whose kinematics in the quasioptical wave beam is determined by field nonuniformity and the ionization frequency that depends on it. Figure 2 illustrates the evolution of the initial stage of the discharge in helium for three pressures ($p = 1$, 3, and 5 torr). We note that the point at which strong, i.e., measureable, emission first occurs is shifted away from the focus and toward the source of the radiation (the shift increases with increasing pressure). The ionization fronts at first propagate in both directions away from point (Fig. 2c), but, very soon, the field becomes screened by the resulting plasma and the photoscan shows only the ionization front facing the incident wave. The velocity of this front depends on the radiation intensity and gas density.

For helium pressures $p \gtrsim 10$ torr and nitrogen pressures $p \gtrsim 2$ torr, secondary ionization fronts were observed during the microwave pulse and were found to propagate against

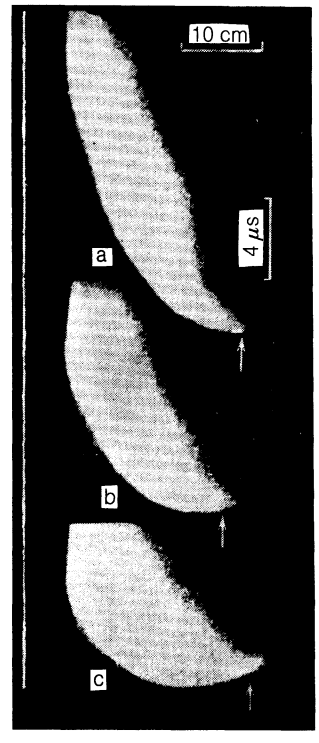

FIG. 2. Optical scan of the helium discharge: a—$p = 1$ torr, b—3 torr, c—5 torr. The beam of radiation propagates from left to right. The time axis points downward. Arrows point to the position of discharge nucleation. The arrow in Fig. 2c should be shifted by 1 cm to the left.

FIG. 3. Optical scan of the helium discharge at $p = 20$ torr.

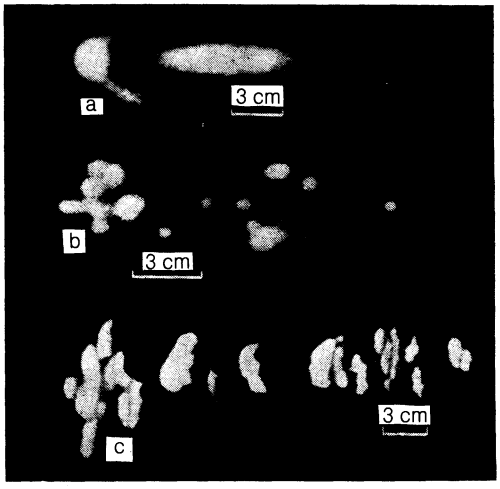

FIG. 4. Photographs of the discharge, recorded in the E plane, using the exposure $\tau_e = 0.2\,\mu$s at different instants of time t from the beginning of the microwave pulse: a—nitrogen, $p = 2$ torr, b—nitrogen, $p = 10$ torr, $t = 90\,\mu$s; c—argon, $p = 50$ torr, $t = 90\,\mu$s.

the radiation with a lower velocity (Fig. 3, He, $p = 20$ torr; the photoscan breaks off on the left because of the limited field of view of the FER).

5. When the discharge dynamics was investigated by high-speed photography, it was found that, as long as the moving ionization front did not approach the boundary of the breakdown region, and was not strongly retarded, its instantaneous photographs (exposure time $\tau_e = 0.2\ \mu$s) showed an emission picture that did not contain small-scale structures of type 2 or 3, shown in Figs. 1b and c. This also applies to the discharge as a whole throughout its existence in the low pressure region, which corresponds to the type 1 structure (see Sec. 3).

Analysis of the instantaneous photographs of the discharge at higher pressures enabled us to examine its fine-scale fragmentation that led to the appearance of type 2 or 3 structures. Depending on pressure, type of gas, and position in the beam, the fine-scale structures seen on the integrating photographs appear either immediately as one whole against the background of quasiuniform emission of the type illustrated in Fig. 4a, or they are formed as a result of the rapid displacement or evolution of initially finer-scale structures that appear against this background. The bright longitudinal bands on the integrating photographs of the discharge in nitrogen and helium (Fig. 1b, type 2 structure) are traces of the individual quasispherical objects (plasmoids) that appear as a result of the fragmentation of the ionization fronts, and propagate toward the microwave radiation. Figure 4 shows instantaneous photographs of the first two ionization waves at low pressure, the plasmoids at intermediate pressure, and the filamentary structure at high pressures. The characteristic time for the nucleation and evolution of small-scale formations in the discharge at $p \sim 10$ torr is $\tau_g \simeq 2$–$3\,\mu$s. The corresponding time at high pressures is probably shorter, but cannot be measured because the shortest time interval between successive frames that could be used in the high-speed photography was $2\,\mu$s.

The evolution of the discharge plasma in the absence of small-scale fragmentation (or the breakdown-wave stage) was also investigated by measuring the electron density. Figure 5 shows the electron density $N(t)$, averaged over the transverse cross section of the breakdown region and recorded with the open resonator at a distance of about 15 cm from the beam focus, for a number of discharges in nitrogen under the same conditions as in Fig. 4a. The maximum density in the first breakdown-wave peak was $N_{max} = 5\times10^{12}$–6×10^{12} cm^{-3} which, under the conditions of this experiment, amounts to 25–30% of the critical value

$$N_c = m(\omega^2+\nu^2)/4\pi e^2 \approx 2\cdot10^{13}\ \text{cm}.$$

At higher pressures ($p > p_1$), the instantaneous photographs and the $N(t)$ curves recorded during the breakdown-wave stage (prior to fragmentation) were found to have the same form as those in Figs. 4a and 5. This correspondence confirms that photographic methods can be used to visualize the discharge structure.

Our results show that the integrated emission observed at our pressures (type 1, 2, and 3 structures) can be identified with three types of discharge in the wave beam, namely, diffuse discharge (continuous), multiplasmoid discharge (with moving spherical quasispherical plasmoids), and filamentary discharge (consisting of a set of fixed filaments).

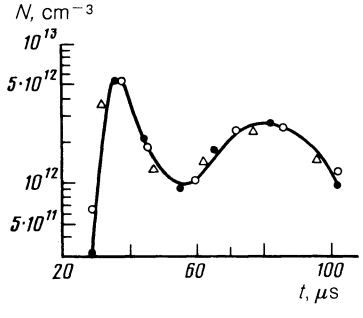

FIG. 5. Time dependence of the electron density in a nitrogen discharge ($p = 2$ torr) at 15 cm from the beam focus. Different points correspond to different discharges.

6. We now turn to the discussion of our results, and begin by considering whether it is possible to describe the evolution of the continuous discharge (without the small-scale structures) by a relatively simple mathematical model[1] in which the field of the axisymmetric wave beam $E(r,z,t)\times\exp[i(\omega t-kz)]$ is described by a parabolic equation that takes into account small-angle refraction, lateral amplitude diffusion, and absorption, and the electron density $N(r,z,t)$ is described by a simple balance equation with a given amplitude dependence of ionization frequency $\nu_i(|E|)\sim|E|^\beta$ and given effective loss frequency $\nu_a=\text{const}$. In terms of dimensionless variables,

$$r/a\to r,\quad z/l\to z,\quad \nu_a t\to t,\quad \mathscr{E}=E/E_c,\quad \tilde{n}=N/N_1 \qquad (1)$$

the corresponding initial set of equations has the form

$$\frac{1}{r}\frac{\partial}{\partial r}\left(r\frac{\partial\mathscr{E}}{\partial r}\right)-2i\left(\frac{\partial\mathscr{E}}{\partial z}+\mu\frac{\partial\mathscr{E}}{\partial t}\right)=\tilde{n}\left(1+i\frac{\nu}{\omega}\right)\mathscr{E}, \qquad (2)$$

$$\frac{\partial\tilde{n}}{\partial t}=(|\mathscr{E}|^\beta-1)\tilde{n}, \qquad (3)$$

where the radial (r) and longitudinal (z) coordinates are measured, respectively, in units of the characteristic lateral (a) and longitudinal ($l=ka^2$) scales of the focal region of the undisturbed beam, $N_1=N_c/kl=N_c\theta^2$, $\theta=(ka)^{-1}$ is the beam convergence angle, $N_c=m(\omega^2+\nu^2)/4\pi e^2$ is the critical density, $\mu=\nu_a l/c$ is a parameter representing the delay of the electromagnetic signal, and E_c is the threshold amplitude, determined by the condition[1)] $\nu_i(E_c)=\nu_a$. Equations (2), and (3) were solved numerically. The initial and boundary conditions were specified so that the concentration was small in the prebreakdown state ($t=0$)

$$N(r,z,0)=N_0=\text{const},\quad \tilde{n}_0=N_0/N_1\ll 1,$$

and the beam was Gaussian and focused at a given distance z_0 from the $z=0$ boundary:

$$\mathscr{E}(r,0,t)=\mathscr{E}_0\exp[-r^2/2(1+iz_0)],\qquad \mathscr{E}_0=\mathscr{E}_m/(1+z_0^2)^{1/4}, \qquad (4)$$

where $\mathscr{E}_m$ is the amplitude of the undisturbed field in the focus. Figures 6a–d show the results of these calculations for the following parameter values: $z_0=1$, $\mathscr{E}_0=1$ ($\mathscr{E}_m=2^{1/2}$), $\beta=4$, $\mu=1$, $\nu/\omega=2\cdot10^{-1}$, $\tilde{n}_0=10^{-4}$. As can be seen, at $t\simeq3$, there is an end to the rapid (avalanche) increase in density in the focal region, which obviously occurs during the initial (not shown in Fig. 6) stage that results from the reduction in the field amplitude (due to refraction in the plasma, associated with the small ν/ω), and the maximum of $\tilde{n}$ begins to move against the beam. The moving ionization front takes the form of an inverted cup (as in Fig. 4a), with its convex surface facing the direction of motion (Fig. 6d). The first soliton-like ionization burst for $t\gtrsim10$ is followed by secondary bursts slower and weaker. The excess of the field amplitude over the breakdown value E_c becomes very small for large t, and the rate of evolution of the discharge becomes very much slower. The maximum value of $\tilde{n}$ in the first ionization peak ($\tilde{n}_{\max}=13.6$) is in good agreement with the approximate estimate[2,14]

$$\tilde{n}_{max}\approx\ln(\tilde{n}_{max}/\tilde{n}_0), \qquad (5)$$

which limits the electron avalanche by refraction for small

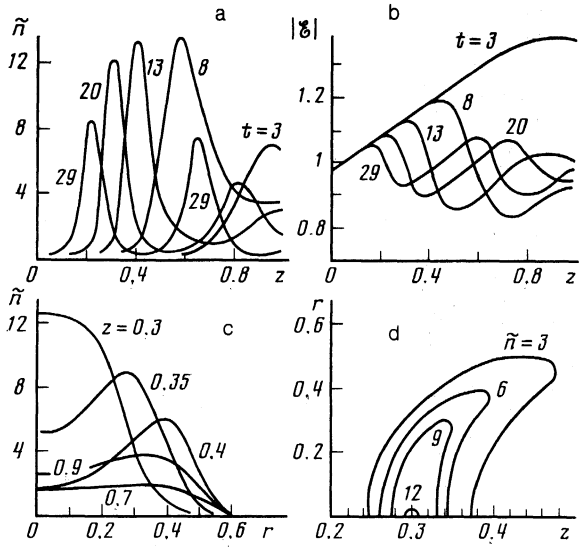

FIG. 6. Evolution of the axial (a,b) and radial (c) distribution of electron density and field amplitude, and lines of constant density for $t=20$(d).

ν/ω, and gives $\tilde{n}_{\max}=11.5$ in the present case. The parabolic equation (2) and the estimate given by (5) are valid for a real beam if the calculated

$$N_{max}=N_1\tilde{n}_{max}=N_c\theta^2\ln(N_{max}/N_0)$$

is small in comparison with N_c, i.e., when

$$\theta^2\ln(N_{max}/N_0)\ll1, \qquad (6)$$

which is more stringent than the simple paraxial condition $\theta\ll1$. We note that, under the conditions of our experiment ($\theta\approx10^{-1}$, $\ln(N_{\max}/N_0)\approx30$), we have $N_{\max}/N_c\approx0.3$, i.e., we can still rely on the qualitative validity of the above theoretical model. On the other hand, the satisfactory agreement between the calculations and the experimental data (shape of ionization front, presence of secondary ionization fronts, and magnitude of $N_{\max}/N_c$) support the validity of the assumptions on which this model is based.

7. The observed fragmentation of the discharge in the wave beam, and its localization in the nodes of the standing wave,[15] can be naturally interpreted in terms of the theory of ionization instabilities in wave fields.[2,16,17] These ideas suggest that the quasistatic (resonance plasma) ionization-field instability[16] predominates in microwave discharges of moderate size, in which stimulated ionization scattering cannot develop for low electron collision frequencies $\nu\ll\omega$. This instability is the ionization analog of the well-known modulation instability of the longitudinal field in plasmas with ponderomotive nonlinearity. It is due to the mutually amplifying effect of perturbations of the longitudinal field (parallel to ∇N) and electron density in transparent plasma ($N<N_c$), and leads (during the the linear stage) to the appearance of layers perpendicular to the field. Generalization of the results reported in Ref. 16, with allowance for electron-electron collisions and electron-ion recombination, leads to the following expression for the maximum growth rate γ of this instability and the corresponding wave number $\varkappa$ of perturbations in the homogeneous discharge (see also Ref. 3):

$$\gamma=\beta A n_s\nu_{is}-2(\beta n_s\nu_{is}Dk^2)^{1/2}-\alpha N_s, \qquad (7)$$

$$\varkappa=(\beta n_s\nu_{is}k^2/D)^{1/4}, \qquad (8)$$

$$A=[1-n_s(1+\nu^2/\omega^2)]\,[(1-n_s)^2+(n_s\nu/\omega)^2]^{-1} \qquad (9)$$

where $\nu_{is}=\nu_a+\alpha N_s$, ν_a is the attachment frequency, α is the recombination coefficient, $\beta=d\ln\nu_i/d\ln|E|\sim 4$–5 is a numerical coefficient representing the slope of the $\nu_i(|E|)$ curve, D is the ambipolar diffusion coefficient, $n_s=N_s/N_c$, and the subscript s labels quantities referring to the unperturbed stationary state.

The high rate of charge-transfer reactions between He^+ and the small ($\sim 1\%$) nitrogen and oxygen impurity ensures that discharges in technical grade helium and nitrogen have similar ionic composition and, consequently, similar values of the dissociative recombination coefficient ($\alpha\simeq 2\times 10^{-8}$–$4\times 10^{-8}$ cm^3/s; Ref. 18). When $\alpha N_s\gg\nu_a$, we have $\nu_{is}\approx\alpha N_s$ and, according to (7),

$$\gamma=\nu_{is}[\beta A n_s-1-2(\beta D k^2/\alpha N_c)^{1/2}]. \qquad (10)$$

For $\nu/\omega\ll(1-n_s)$, where $A\simeq 1/(1-n_s)$, the instability ($\gamma>0$) occurs when

$$\beta n_s/(1-n_s)>1+2(\beta D k^2/\alpha N_c)^{1/2}. \qquad (11)$$

The wave number $\varkappa$ at the instability threshold ($\gamma=0$) is given by

$$\varkappa_c=k\left[\frac{2\beta n_s(1-n_s)}{n_s(\beta+1)-1}\right]^{1/2}>k[2(1-n_s)]^{1/2}. \qquad (12)$$

For $n_s=n_{s\max}\approx 30\,\theta^2$, which is reached in a "smooth" discharge [see (5)], condition (11) determines the threshold pressure p_1 for given $D(p)$ (when $p<p_1$, the instability is suppressed by diffusion). The values of p_1 estimated in this way for discharges in helium and nitrogen are found to lie precisely in the pressure range in which the transition from the diffuse discharge to the multiplasmoid discharge is observed.

In argon at moderate pressure, the absence of fast charge transfer and conversion ensure that the atomic ion recombines to form Ar_2^+, which has a low recombination coefficient ($a\leqslant 10^{-10}$ cm^3/s).[19] Even for $n_s=n_{s\max}$, estimates show that the condition $\gamma>0$ is not satisfied at any pressure in this case (it can be satisfied with some difficulty for $\nu/\omega>1$ for which another type of instability, examined below, plays the leading part). This can be used to explain type 2 structures in argon.

We note that, when the growth rate (7) is positive, the instability does not arise if the linear dimensions of the discharge region do not exceed the stratification period $2\pi/\varkappa$. This situation was probably realized in the experiments reported in Ref. 6, in which the dimensions of the focal region of the beam were smaller than or the same as λ, and the type 2 structure was not seen at all.

The above linear theory of instability does not describe the evolution of a discharge with well-developed perturbations. The multiplasmoid discharge observed in our experiment is probably associated with the nonlinear stage of instability. The study of this instability in a real (inhomogeneous and nonstationary) discharge in a wave beam is a very complicated problem that has not been adequately tackled so far. Nevertheless, we note the satisfactory agreement between experimental data and the predictions of the linear theory for the order of magnitude of the characteristic instability development time ($\gamma_{\max}^{-1}\simeq 2\times 10^{-6}$ s) and the characteristic instability scale ($\Lambda_c=2\pi/\varkappa_c\simeq 1$ cm), which probably corresponds to the threshold value of the density determined from (11).

For $\nu\gtrsim\omega$, the discharge is dominated by another instability, namely, the ionization-heating instability,[17] which arises from the mutual amplification of electron-density and gas-temperature perturbations and leads to the decay of the discharge into filaments running parallel to the field. In our experiment, the gas pressure $p=p_2$ determined from the condition $\nu(p_2)=\omega$ lies in the region of the transition to a filamentary discharge, frequently observed in this pressure range ($\nu>\omega$) in previous experiments.[4,6,15,20] The growth rate $\gamma_t\simeq(\beta\gamma_0\nu_{is})^{1/2}$ of this instability (γ_0 is the reciprocal time for the uniform heating of the gas) is 10^6–10^7 s^{-1} according to estimates for $p\gtrsim 100$ torr. Its optimum scale $\Lambda=2\pi/\varkappa$ (separation between filaments) is determined by (8), as in the preceeding case; when $p\sim 100$ torr, this yields $\Lambda\sim 0.1$–0.3 cm, which is in qualitative agreement with experiment.

It is important to note that the field amplification effect on plasmoid boundaries, which occurs at right angles to them, may play an important part in the formation of the filamentary structure for $\nu>\omega$, since it produces a rapid expansion of the plasmoid in the direction of the field **E**. We note that this effect can probably also be used to explain the "branched discharge" consisting of a large number of randomly branched luminous filaments[6,7,12] at pressures $p\sim 1$ atm. A more detailed explanation of this and other fast processes in fragmenting discharges will require, on the one hand, further theoretical investigation and, on the other, the use of faster and more sensitive recording systems.

[1] V. B. Gil'denburg, **40**, 215 (1979).
[2] V. B. Gil'denburg, *Nonlinear Waves: Propagation and Interactions* [in Russian], Nauka, Moscow, 1981, p. 87.
[3] A. L. Vikharev, V. B. Gil'denburg, A. G. Litvak, and V. E. Semenov, *Abstract of Papers, 13th All-Union Conf. on Radiowave Propagation* [in Russian], Nauka, Moscow, **1**, 119 (1981).
[4] J. Allison, A. L. Cullen, and A. Zavody, Nature, **193**, 72 (1962).
[5] N. A. Bogatov, Yu. V. Bykov, N. P. Benediktov, *et al.*, Fiz. Plasmy. **12**, 725 (1986) [Sov. J. Plasma Phys. **12**, 416 (1986)].
[6] L. P. Grachev, I. I. Esakov, G. I. Mishin, *et al.*, Zh. Tekh. Fiz. **55**, 389 (1985) [Sov. Phys. Tech. Phys. **30**, 228 (1985)].
[7] G. M. Batanov, S. P. Gritsinin, I. A. Kossii *et al.*, Trudy FIAN, **160**, 174 (1985).
[8] W. E. Scharfman, W. C. Taylor, and T. Morita, IEEE Trans. **12AP**, 709 (1964).
[9] Yu. A. Lapan, Zh. Tekh. Fiz. **46**, 2321 (1976) [Sov. J. Tech. Fiz. **21**, 1367 (1976)].
[10] W. M. Bollen, C. L. Yee, A. W. Ali *et al.*, J. Appl. Phys. **54**, 101 (1983).
[11] M. M. Butslov, B. M. Stepanov, and S. D. Fanchenko, *Electron–Optical Converters and Applications in Science Research* [in Russian], Nauka, Moscow, 1978.
[12] A. L. Vikharev, V. B. Gil'denburg, O. A. Ivanov, and A. N. Stepanov, Fiz. Plazmy **10**, 792 (1984) [Sov. J. Plasma Fiz. **10**, 460 (1984)].
[13] Yu. P. Raĭzer, Laser-Induced Discharge Phenomena, Consultants Bureau, New York (1977).
[14] V. B. Gil'denburg, Zh. Eksper. Teor. Fiz. **78**, 952 (1980) [Sov. Phys.–JETP **51**, 480 (1980)].
[15] A. L. Vikharev, V. B. Gil'denburg, O. A. Ivanov, and A. N. Stepanov, Fiz. Plazmy, **10**, 165 (1984) [Sov. J. Plasma Phys. **10**, 96 (1984)].
[16] V. B. Gil'denburg, and A. V. Kim, Zh. Eksper, Teor. Fiz. **74**, 141 (1978) [Sov. Phys. JETP **47**, 72 (1978)].
[17] V. B. Gil'denburg, and A. V. Kim, Fiz. Plazmy **6**, 904 (1980) [Sov. J. Plasma Phys. **6**, 496 (1980)].
[18] A. V. Eletskiĭ and B. M. Smirnov, Usp. Fiz. Nauk **136**, 25 (1982) [Sov. Phys. Uspekhi **25**, 13 (1982)].
[19] E. W. McDaniel, Collision Phenomena in Ionized Gases, Wiley, 1964.
[20] Yu. V. Bykov, S. V. Golubev, A. L. Goldenberg and V. G. Zorin, Zh. Tekh. Fiz. **54**, 723 (1984) [Sov. Phys. Tech. Phys. **29**, 428 (1984)].
[21] V. M. Batenin, P. P. Klimovskiĭ and V. R. Khamrev. Zh. Exsper. Teor. Fiz. **71**, 603 (1976) [Sov. Phys. JETP **44**, 316 (1976)].

Translated by S. Chomet